

On the fracture toughness and stable crack growth in shape memory alloy actuators in the presence of transformation-induced plasticity

S. Jape  · T. Baxevanis · D. C. Lagoudas

Received: 22 March 2017 / Accepted: 7 September 2017 / Published online: 20 September 2017
© Springer Science+Business Media B.V. 2017

Abstract The effect of transformation-induced plasticity (TRIP) on the fracture response of polycrystalline shape memory alloys is analyzed in the prototype infinite center-cracked plate subjected to thermal cycling under constant mechanical loading in plain strain. Finite element calculations are carried out to determine the mechanical fields and the crack-tip energy release rate using the virtual crack closure technique. Similar to phase transformation, TRIP is found to affect both the driving force for crack growth and the crack growth kinetics by promoting crack advance when occurring in a fan in front of the crack tip and providing a “shielding” effect when occurring behind that fan. Accumulation of TRIP strains over the cycles results in higher energy release rates from one cycle to another and may result in crack growth if the crack-tip energy release rate reaches a material “specific” critical value after a sufficient number of cycles. During crack advance, the shielding effect of the TRIP strains left in the wake of the growing crack dominates and therefore TRIP is

found to both promote the initiation of crack growth and extend the stable crack growth regime.

Keywords Shape memory alloys · Fracture toughness · Crack growth · TRIP · Transformation toughening · VCCT

1 Introduction

Shape memory alloys (SMAs) are capable of recovering seemingly permanent, large deformations when subjected to appropriate mechanical or thermal loads owing to a diffusionless, solid-to-solid, austenite-to-martensite phase transformation (Kumar and Lagoudas 2008). As such, solid-state SMA actuators are a potential alternative to traditional electromagnetic actuators in applications where a small volume and/or large actuation force is required and thermodynamic efficiency is not essential (Hartl and Lagoudas 2007; Sreekumar et al. 2007; Nespoli et al. 2010).

When utilized as solid-state actuators, SMAs are generally subjected to thermomechanical (actuation) loading cycles that develop permanent deformations originating from the stressed transition layer between the austenite and martensite phases. This stress drives dislocation activity resulting in TRIP (Bo and Lagoudas 1999d). Generation and accumulation of TRIP over the cycles (Perkins and Bobowiec 1986; Liu and McCormick 1994; Cherkaoui et al. 1998; Fischer et al. 2000) has a strong impact on the macroscopic ther-

S. Jape · D. C. Lagoudas
Department of Aerospace Engineering, Texas A&M University, College Station, TX 77843, USA
e-mail: sameer137@tamu.edu

T. Baxevanis (✉)
Department of Mechanical Engineering, University of Houston, Houston, TX 77204, USA
e-mail: tbaxevanis@uh.edu

D. C. Lagoudas
Department of Materials Science and Engineering, Texas A&M University, College Station, TX 77843, USA
e-mail: lagoudas@tamu.edu

momechanical deformation response of SMAs, affecting the critical stress required for phase transformation, maximum transformation strain, transformation hardening, and width of the hysteresis loop, and in turn is expected to strongly influence the SMA fracture response. Thus, an understanding of the effect of TRIP on the fracture response of these materials is imperative for the effective design of high-performing and durable solid-state SMA actuators.

Fracture in SMAs is influenced, apart from TRIP, by the reversibility of phase transformation, the associated absorption/release of heat, and the reorientation and detwinning of martensite variants; thus, it is more complex than the fracture response of conventional metallic materials. A considerable amount of experimental and theoretical research has been dedicated toward addressing the problem of crack initiation and growth in SMAs under mechanical loading at nominally isothermal conditions (Birman 1998; Gall et al. 2001; Wang et al. 2005; Yan and Mai 2006; Daymond et al. 2007; Robertson et al. 2007; Daly et al. 2007; Creuziger et al. 2008; Desindes and Daly 2010; Maletta and Furgiuele 2010, 2011; LExcellent et al. 2011; Hazar et al. 2015; Ardakani et al. 2015). It has been observed that formation of stress-induced martensite restricts the extent of plastic yielding at the crack-tip (Gall et al. 2001; Gollerthan et al. 2009; Robertson et al. 2007; Baxevanis and Lagoudas 2012; Baxevanis et al. 2012; Ungár et al. 2017) while stress redistribution, resulting from the transformed material left in the wake of an advancing crack, is mostly responsible for the observed stable crack growth (Stam and Giessen 1995; Yi and Gao 2000; Yi et al. 2001; Freed and Banks-Sills 2007; Robertson et al. 2007; Baxevanis et al. 2013a, 2014, 2013b). The ASTM standards are not adequate for determining a configuration-independent driving force for crack growth on the basis of the load–load line displacement, as they do not account for the transformation-induced changes in the apparent elastic properties; recently Maletta et al. (2016) used Digital Image Correlation (DIC) to calculate the crack-tip Stress Intensity Factor (SIF) under isothermal loading at various temperatures. The fracture response of SMAs under combined thermo-mechanical (actuation) loading has also been addressed recently (Jape et al. 2014, 2015; Baxevanis et al. 2016; Jape et al. 2016). It has been demonstrated that the driving force for crack growth may increase substantially during cooling under constant mechanical loading and result in crack

advance (Baxevanis et al. 2016) due to stress redistribution caused by “global” scale transformation in front of the crack (Budiansky et al. 1983; Lambropoulos 1986). Stable crack growth was further observed which should be attributed to stress redistribution caused by the transformed material left in the wake of the advancing crack (Jape et al. 2016). In the present work, the aforementioned finite element analysis of the fracture response of SMAs under actuation type loading is extended to include TRIP, utilizing a modified material constitutive law developed by Bo and Lagoudas (1999a, b, c); Entchev and Lagoudas (2004). The numerical results delve into the details of the evolution of mechanical fields close to the crack tip, the driving force for crack growth, and crack growth kinetics.

The paper is organized as follows. Section 2 reviews the phenomenological constitutive model for polycrystalline SMAs that includes TRIP. In Sect. 3, the boundary value problem of an infinite center-cracked SMA plate subjected to combined cyclic thermomechanical loading under plane strain is formulated. In Sect. 4, numerical results for static and advancing cracks are presented, followed by a summary of the key findings in Sect. 5.

2 Material constitutive model

The constitutive model is that proposed by Bo and Lagoudas, which is an extension of the constitutive model for polycrystalline SMAs undergoing solid-state diffusionless phase transformation developed by Boyd and Lagoudas (1996).

Additive decomposition of the total strain tensor in an elastic, a transformation, and a plastic part is assumed and the classical, rate-independent, small-strain flow theory framework for the evolution of inelastic strains is adopted. Thus, the increments of the strain tensor components $d\varepsilon_{ij}$ are given as

$$d\varepsilon_{ij} = S_{ijkl}d\sigma_{kl} + dS_{ijkl}\sigma_{kl} + d\varepsilon_{ij}^t + d\varepsilon_{ij}^p, \quad (1)$$

where σ_{ij} , ε_{ij}^t , ε_{ij}^p are the Cartesian components of the stress tensor, transformation strain tensor, and plastic strain tensor, respectively, and S_{ijkl} are the components of the “current” compliance tensor. Throughout this paper, standard Einstein notation is used with summation over repeated indices assumed. The current compliance tensor varies with the martensitic volume fraction ξ as $S_{ijkl} = (1 - \xi)S_{ijkl}^A + \xi S_{ijkl}^M$, where S_{ijkl}^A and

S_{ijkl}^M are the components of the compliance tensor of austenite and martensite, respectively. In this paper, it is assumed that both austenite and martensite are isotropic and $S_{ijkl}^\alpha = \frac{1+\nu_\alpha}{2E_\alpha}(\delta_{il}\delta_{jk} + \delta_{ik}\delta_{jl}) - \frac{\nu_\alpha}{E_\alpha}\delta_{ij}\delta_{kl}$, where the index α stands for A in the case of austenite and for M in the case of martensite. E_α, ν_α denote the Young's modulus and Poisson's ratio, respectively, of the two phases and δ_{ij} is Kronecker's delta.

The plastic strain considered here is different from conventional plasticity in metals. Due to the misfit between the austenite–martensite interfaces, significant distortion is created. In addition, in a polycrystalline SMA, different grains transform in different manners, which causes additional distortion at the grain boundaries. These two phenomena act in concert, and the final result is an observable macroscopic plastic strain, which occurs at effective stress levels much lower than the plastic yield limit of the material without phase transformation. This model does not address the plastic strain evolution initiated when pure austenite or martensite is subjected to effective stresses that exceed the critical stress for slip, but is focused on plasticity caused by cyclic transformation only.

2.1 Evolution of transformation strains

An evolution equation of the transformation strain is defined so that it is related to the evolution of martensite volume fraction, ξ ,

$$d\varepsilon_{ij}^t = \Lambda_{ij}d\xi, \quad \Lambda_{ij} = \begin{cases} \frac{3}{2} \frac{H^{cur}(\bar{\sigma})}{\bar{\sigma}} s_{ij}, & d\xi > 0, \\ \frac{\varepsilon_{ij}^t}{\xi}, & d\xi < 0, \end{cases} \quad (2)$$

where Λ_{ij} are the components of the direction tensor. Here, $H^{cur}(\bar{\sigma})$ is the uniaxial transformation strain magnitude for complete transformation, $\bar{\sigma} = \sqrt{\frac{3}{2}s_{ij}s_{ij}}$ is the Mises equivalent stress, and $s_{ij} = \sigma_{ij} - \sigma_{kk}\delta_{ij}/3$ are the stress deviator components. During forward transformation, the transformation strain is oriented by the direction of the deviatoric stress, which motivates the selected J_2 form of the direction tensor. During reverse phase transformation, it is assumed that the direction and magnitude of the transformation strain recovery is governed by the average orientation of the martensite at transformation reversal (the cessation of forward transformation, be it partial or full). This defi-

nition allows the transformation strain to return to zero for every state with a null martensite volume fraction.

$H^{cur}(\bar{\sigma})$ is a function of the stress state since most SMA materials do not exhibit a constant maximum attainable transformation strain at all stress levels. A saturated value of maximum attainable transformation strain, H^{max} , is reached at a high stress level, which is dependent on the SMA material as well as the processing conditions for a polycrystalline material, resulting in different crystallographic and morphological textures, for example. Following this observation, the maximum transformation strain $H^{cur}(\bar{\sigma})$ is represented by the following decaying exponential function

$$H^{cur}(\bar{\sigma}) = H^{max} \left(1 - e^{-k\bar{\sigma}}\right), \quad (3)$$

where the parameter k controls the rate at which $H^{cur}(\bar{\sigma})$ exponentially evolves from 0 to H^{max} . As the saturation value of the maximum transformation strain evolves with the number of cycles, its evolution is assumed to obey the following equation

$$H^{max} = (H)^{fin} + \left[(H)^{init} - (H)^{fin}\right] e^{-\lambda_1 \zeta^d}, \quad (4)$$

where $(H)^{fin}$ and $(H)^{init}$ are the final and initial values, and λ_1 is a positive material constant that governs the increasing rate of H^{max} .

2.1.1 Evolution of plastic strains

Similar to the evolution of transformation strain, the direction of plastic strain is determined by the direction of the applied stress. The development of the plastic strain is connected to the detwinned martensitic volume fraction, $\xi^d = \frac{H^{cur}(\bar{\sigma})}{H^{max}}\xi$, as

$$d\varepsilon_{ij}^p = \Lambda_{ij}^p d\xi, \quad \Lambda_{ij}^p = \begin{cases} \frac{3}{2} C_1^p \frac{H^{cur}(\bar{\sigma})}{H^{max}} \frac{s_{ij}^{eff}}{\bar{\sigma}^{eff}} e^{-\frac{\zeta^d}{C_2^p}}, & d\xi > 0 \\ C_1^p \frac{H^{cur}(\bar{\sigma})}{H^{max}} \frac{\varepsilon_{ij}^t}{\xi} e^{-\frac{\zeta^d}{C_2^p}}, & d\xi < 0, \end{cases} \quad (5)$$

where Λ_{ij}^p are the components of the direction tensor,

$$\zeta^d = \int_0^t \frac{H^{cur}(\bar{\sigma})}{H^{max}} |\dot{\xi}| d\tau \quad (6)$$

is the accumulated detwinned martensite volume fraction, s_{ij}^{eff} are the components of the deviatoric part of

the effective stress tensor, which is defined as $\sigma_{ij}^{eff} = \sigma_{ij} + \beta_{ij}$ and β_{ij} are the components of the back stress that is introduced below. The material parameters C_1^p and C_2^p govern the saturation value of the plastic strain as well as the number of cycles necessary for its saturation.

The components of the back stress β_{ij} , which control the kinematic portion of the plastic hardening, are assumed to have the following polynomial functional representation

$$\beta_{ij} = \frac{\varepsilon_{ij}^t}{\bar{\varepsilon}^t} \sum_{i=1}^{N^b} D_i^b [H^{cur}(\bar{\sigma}) \xi]^{(i)}, \tag{7}$$

where N^b is the degree of the polynomial and D_i^b are the coefficients associated with the back stress. The latter coefficients are assumed to change with the evolution of the accumulated detwinned martensitic volume fraction ζ^d as

$$D_i^b = (D_i^b)^{fin} + [(D_i^b)^{init} - (D_i^b)^{fin}] e^{-\lambda_1 \zeta^d}, \tag{8}$$

where $(D_i^b)^{fin}$ and $(D_i^b)^{init}$ are the final and initial values of D_i^b , and λ_1 is a positive material constant that governs the increasing rate of D_i^b . Note that in the present model, the change of H^{max} is assumed to obey the same governing equation as the change of D_i^d .

2.1.2 Evolution of martensitic volume fraction

The evolution of the martensitic volume fraction can be inferred from the transformation surface

$$\Phi = 0, \quad \Phi = \begin{cases} \pi - Y, & d\xi > 0, \\ -\pi - Y, & d\xi < 0, \end{cases} \tag{9}$$

where

$$\pi = \sigma_{ij}^{eff} \Lambda_{ij} + \sigma_{ij} \Lambda_{ij}^p + \frac{1}{2} \Delta S_{ijkl} \sigma_{ij} \sigma_{kl} + \eta(\xi) + \rho \Delta s_0 (T - M^{0s}) + Y. \tag{10}$$

In the above equation,

$$M^{0s} = T_0 + \frac{1}{\rho \Delta s_0} (Y + \rho \Delta u_0) \tag{11}$$

is the initial martensitic-start temperature, s_0 and u_0 are the specific entropy and internal energy, respectively, ρ is the density, Δ denotes the difference in property

between the martensitic and the austenitic states, Y is a material constant representing a measure of the internal dissipation during phase transformation, and

$$\eta = -D_1^d [-\ln(1 - \xi)]^{\frac{1}{m_1}} + D_2^d \xi \tag{12}$$

is the drag stress that accounts for the isotropic hardening. The latter coefficients are assumed to change with the evolution of the accumulated detwinned martensitic volume fraction ζ^d as

$$D_i^d = (D_i^d)^{fin} + [(D_i^d)^{init} - (D_i^d)^{fin}] e^{-\lambda_2 \zeta^d}, \tag{13}$$

where $(D_i^d)^{fin}$ and $(D_i^d)^{init}$ are the final and initial values of the parameter, and λ_2 is a positive material constant governing the evolution of D_i^d . The equations governing the change of Y , M^{0s} , and $\rho \Delta s_0$ are assumed similar to (13)

$$Y = (Y)^{fin} + [(Y)^{init} - (Y)^{fin}] e^{-\lambda_2 \zeta^d}, \tag{14}$$

$$M^{0s} = (M^{0s})^{fin} + [(M^{0s})^{init} - (M^{0s})^{fin}] e^{-\lambda_2 \zeta^d}, \tag{15}$$

$$\rho \Delta s_0 = (\rho \Delta s_0)^{fin} + [(\rho \Delta s_0)^{init} - (\rho \Delta s_0)^{fin}] e^{-\lambda_2 \zeta^d}. \tag{16}$$

Constraints on the evolution of ξ are expressed in terms of the Kuhn–Tucker conditions given for forward and reverse phase transformation as

$$d\xi \geq 0, \quad \Phi \leq 0, \quad \Phi d\xi = 0 \tag{17}$$

$$d\xi \leq 0, \quad \Phi \leq 0, \quad \Phi d\xi = 0. \tag{18}$$

As evident in Fig. 1 in which simulations of the stress–strain response under uniaxial mechanical cyclic loading and of the strain–temperature response during thermal cycling under a constant bias load are plotted, the constitutive law can reproduce several characteristic changes of the progressive evolution of the hysteresis loop in addition to the evolution of the TRIP strain, i.e., (i) decrease of the stress level required for the onset of transformation, (ii) increase of the transformation hardening, (iii) decrease of the width of the hysteresis loop, and (iv) decrease of the maximum transformation strain. Parameter values for the SMA matrix material used in the present analysis are given in Table 1.

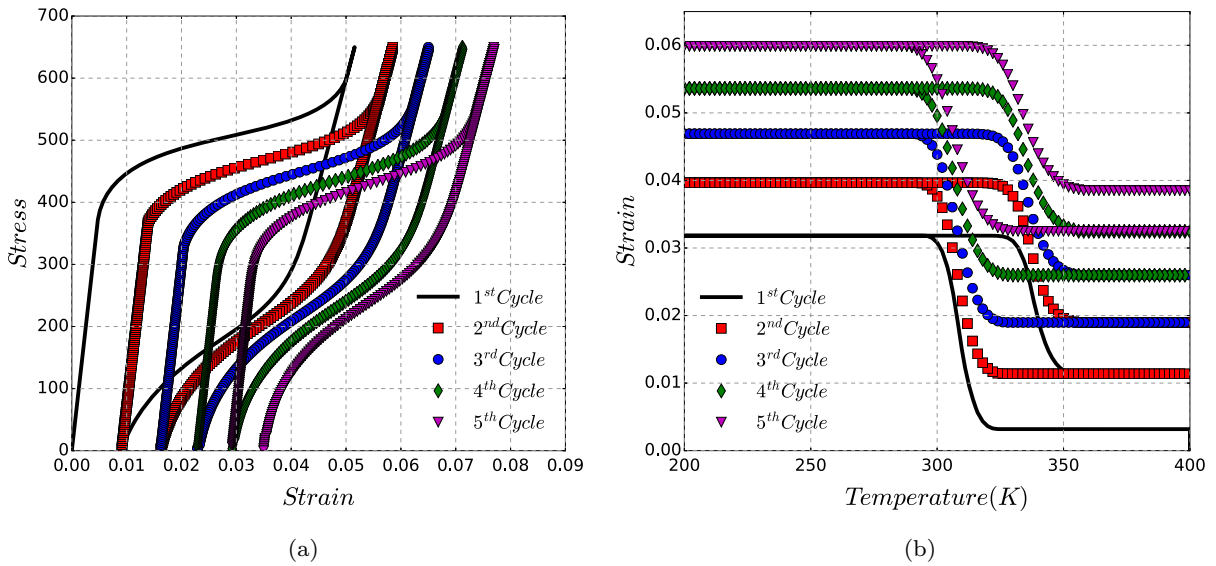


Fig. 1 Uniaxial deformation response. **a** Stress–strain response under mechanical cycling at a constant nominal temperature, and **b** strain–temperature response during thermal cycling under constant bias load

Table 1 Parameter values

Parameter	Value
<i>(a) Elastic constants</i>	
E_A (MPa)	70,000
ν_A	0.33
E_M (MPa)	30,000
ν_M	0.33
<i>(b) Transformation and plastic deformation constants</i>	
M^{0s} [K]	311.0
H^{max}	0.069
D_1^b (MPa)	3.4×10^3
D_2^b (MPa)	-2.23×10^5
D_3^b (MPa)	8.32×10^6
D_4^b (MPa)	-1.50×10^8
D_5^b (MPa)	1.03×10^9
D_1^d (MPa)	3.4×10^3
D_2^d (MPa)	3.4×10^3
C_1^p	0.0036
C_2^p	18

3 Formulation of the boundary value problem

In this section, a brief description of the boundary value problem of an infinite center-cracked SMA plate

subjected to constant, uniaxial mode-I tensile load at the far-field boundaries and thermal cycling is given (Fig. 2). A system of co-ordinates (x_1, x_2, x_3) is chosen with origin at the center of the crack, x_1 -axis extending parallel to the crack faces, x_2 parallel to the direction of loading and x_3 along the thickness of the specimen. The SMA panel is considered to be thick enough so that plane strain conditions hold, and an analysis is performed in the (x_1, x_2) plane.

The mechanical load is applied at a constant ambient temperature, T_h , which is assumed greater than the austenitic-finish temperature, A_f , and lower than M_d , so that phase transformation will take place at sufficient load levels. The resulting uniaxial tensile stress at infinity, σ_∞ , is assumed sufficiently smaller than the stress required for initiation of martensitic transformation, σ^{M_s} , at the given temperature T_h so that small scale transformation conditions prevail, according to which the size of the transformation zone is small compared to the crack length $2a$. Moving from the boundary inwards to the crack tip, a region of partially transformed material will be first encountered, and a region of fully transformed material will be found closer to the crack tip. Then the temperature is cycled between T_h and a temperature T_c , which is lower than the martensitic-finish temperature, M_f , to ensure that the entire material is transformed from austenite to martensite at the end of cooling (Fig. 3). The temperature distribution

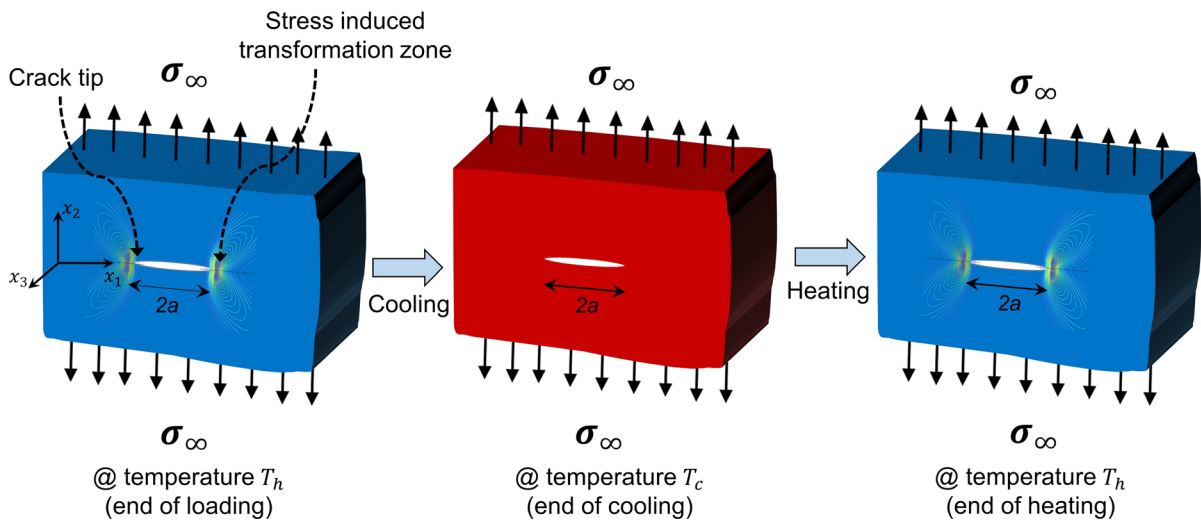


Fig. 2 Boundary value problem for an infinite center-cracked SMA plate initially in the austenite phase subjected to a thermal cycle under a constant far-field uniaxial tensile load. Martensite regions are shown in red and austenite ones in blue

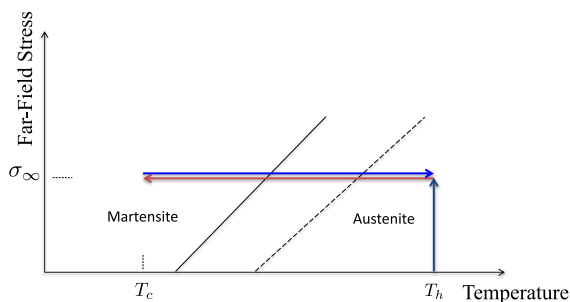


Fig. 3 Isobaric actuation loading path: constant uniaxial tensile load followed by cooling and heating. At the end of cooling the whole material is in the martensite state (left of the solid line) while at the end of heating it is the austenite state (right of the dashed line)

is assumed uniform throughout the material at every instant, i.e., latent heat effects are neglected by assuming that the rates of both the mechanical and thermal loading are sufficiently slow with respect to the time rate of heat transfer by conduction. In real applications of SMA components, the generation of entropy and heat during phase transformation may violate this assumption, influencing the phase transition stress-values that are temperature dependent and in turn the fracture response of SMAs due to the resulting strong thermomechanical coupling. The effect of latent heat on the driving force for crack growth during thermal actuation of SMAs will be examined in a subsequent publication.

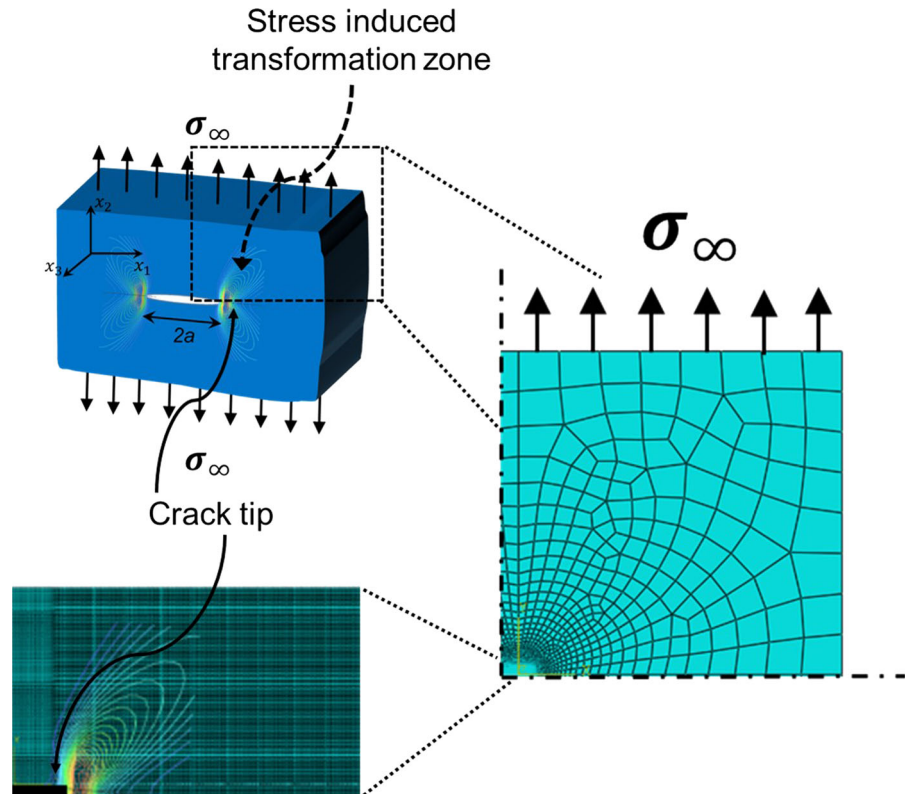
Only half of the infinite domain is analyzed due to symmetry of the problem and only a quarter is plotted due to symmetry of stress and transformation fields across the crack line (Fig. 4). The ABAQUS finite element suite is employed, and the finite element mesh consists of 4-node bilinear plane strain quadrilateral elements with reduced integration, hourglass control, and finer mesh density in the crack growth region in front of the crack tip. Virtual Crack Closure Technique (VCCT) ([47]), which is based on Irwin's crack closure integral (Irwin 1958; Rybicki and Kanninen 1977; Krueger 2004; Xie and Biggers 2006), is used to calculate the driving force for crack growth, which is appropriately approximated by the crack-tip energy release rate. The validity of the assumed fracture parameter as a single parameter capable of describing the mechanical fields close to the crack tip, and of the VCCT methodology in calculating it, has been established in previous investigations (Baxevanis et al. 2016; Jape et al. 2016).

4 Results

4.1 Mechanical fields close to stationary cracks

Some features of the crack-tip mechanical fields are now presented. Contours of martensite volume fraction and TRIP during thermomechanical loading are presented in Figs. 5 and 6. The size of the stress-induced

Fig. 4 Finite element discretization of the domain of integration



martensitic zone resulting from the applied mechanical load prior to cooling complies with the small scale transformation assumption adapted for the calculations. During cooling, transformation occurs first in a fan in front of the crack tip and expands to regions behind the crack tip as the temperature decreases. During heating, reverse phase transformation occurs first behind the crack tip, where the stress levels are lower and in regions in front of the crack tip at higher values of temperature. The evolution of TRIP strains—being a byproduct of phase transformation either forward or reverse—closely follows that of the transformation zone, increasing in magnitude as the phase transformation zone expands or shrinks during cooling or heating, respectively, and accumulates over the thermal cycles. The thermomechanically-induced phase transformation and TRIP strains result in a stress redistribution that changes the crack-tip stress field, as shown in Figs. 7 and 8, in which the von Mises stress and mean normal stress, $\sigma_m = 1/3 \cdot (\sigma_{11} + \sigma_{22} + \sigma_{33})$, distributions at the crack tip prior to thermal cycling (i.e., at $T = T_h$) and at the end of cooling (i.e., at $T = T_c$) are presented.

4.2 Energy release rate during thermal cycling under a constant applied load

The effect of thermomechanically-induced phase transformation on the driving force for crack growth during thermal cycling under constant applied load, as given by the ratio G_I/G_∞ , is examined next, where G_∞ corresponds to the value of the energy release rate due to the mechanical load alone, i.e., at $T = T_h$ prior to thermal cycling.

As shown in Fig. 9, during the first cooling cycle, the energy release rate initially increases until it reaches a peak and then decreases before attaining a constant value once the entire material is fully transformed. During heating, the energy release rate starts initially increasing once reverse phase transformation initiates, then, after reaching a peak, it decreases before attaining, eventually, a constant value. The peak value is about an order of magnitude higher than that at the beginning of thermal cycling. In subsequent thermal cycles, the driving force displays a similar behavior with higher peak driving forces in every thermal cycle.

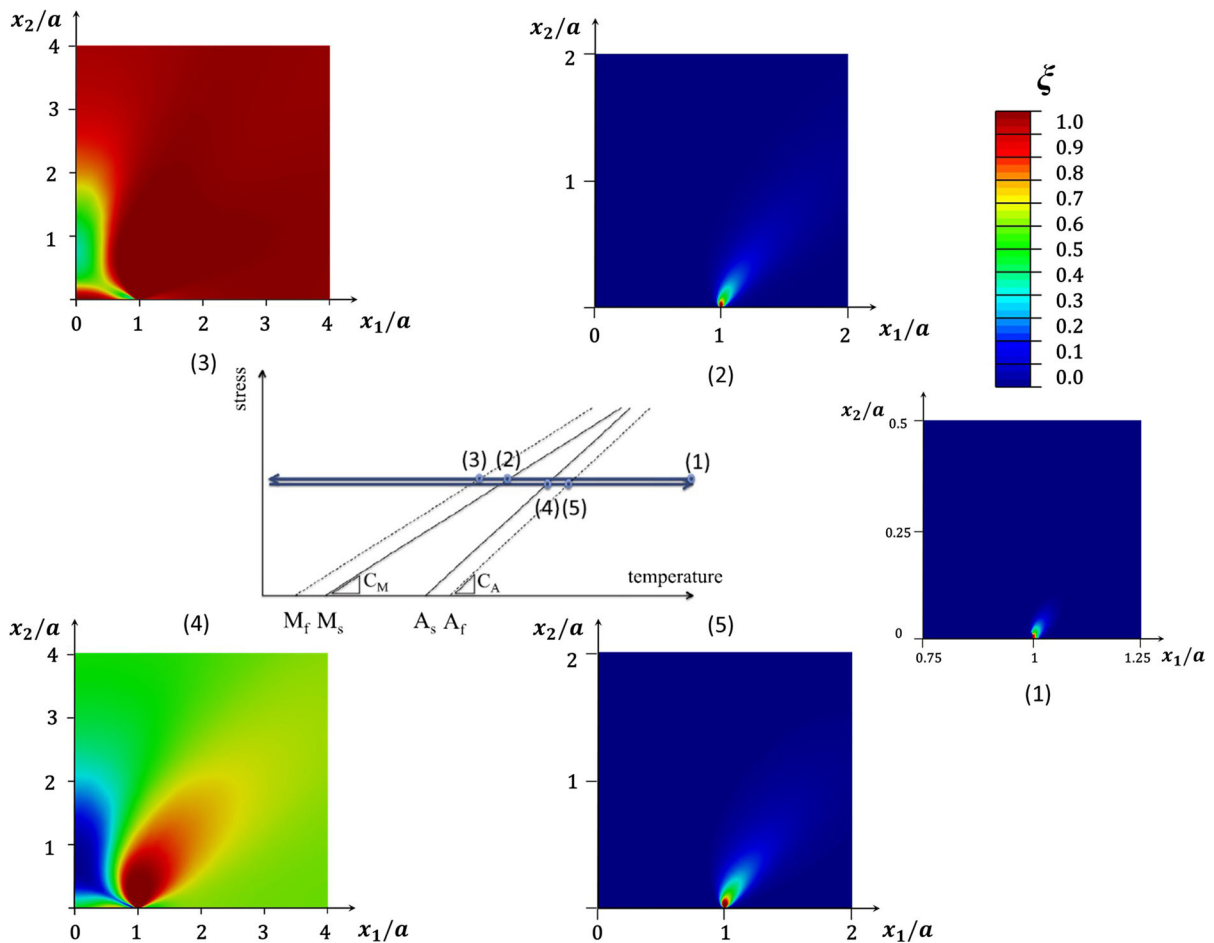


Fig. 5 Contours of martensite volume fraction ξ at different temperatures numbered on the stress–temperature phase diagram during the actuation loading. Note that the near-tip regions in which martensite volume fraction is depicted are of different sizes

An insight into the presented results concerning the effect of actuation on the crack-tip energy release rate, G_I/G_∞ , has already been given in previous investigations by Budiansky et al. (1983), Lambropoulos (1986), Baxevanis et al. (2016), Jape et al. (2016); stress redistribution due to “global”-scale transformation and TRIP occurring in regions “in front” of the crack tip results in raising the driving force for crack growth, while stress redistribution due to transformation and TRIP taking place “behind” the crack tip results in crack shielding. Thus, during cooling, transformation and TRIP strains occurring initially in a fan in front of the crack raise the driving force for crack growth. The subsequent decrease of the driving force for crack growth once the peak is reached should then be attributed to transformation and result-

ing TRIP strains occurring in regions behind the crack tip that have the opposite effect of shielding the crack. A similar argument can explain the behavior of the crack-tip energy release rate during heating. The material first reverse transforms in regions behind the crack tip where the stresses are low, and the shielding effect of the transformation strains in those regions is lost. The outcome is an increase in the driving force for crack growth although the TRIP strains, at the same time, increase in magnitude in these regions providing shielding, since the magnitude of the transformation strains remains an order of magnitude greater than that of TRIP strains for tens/hundreds of thermal cycles. Then the material reverse transforms in regions in front of the crack tip and the anti-shielding effect of the transformation strains is diminished, resulting in

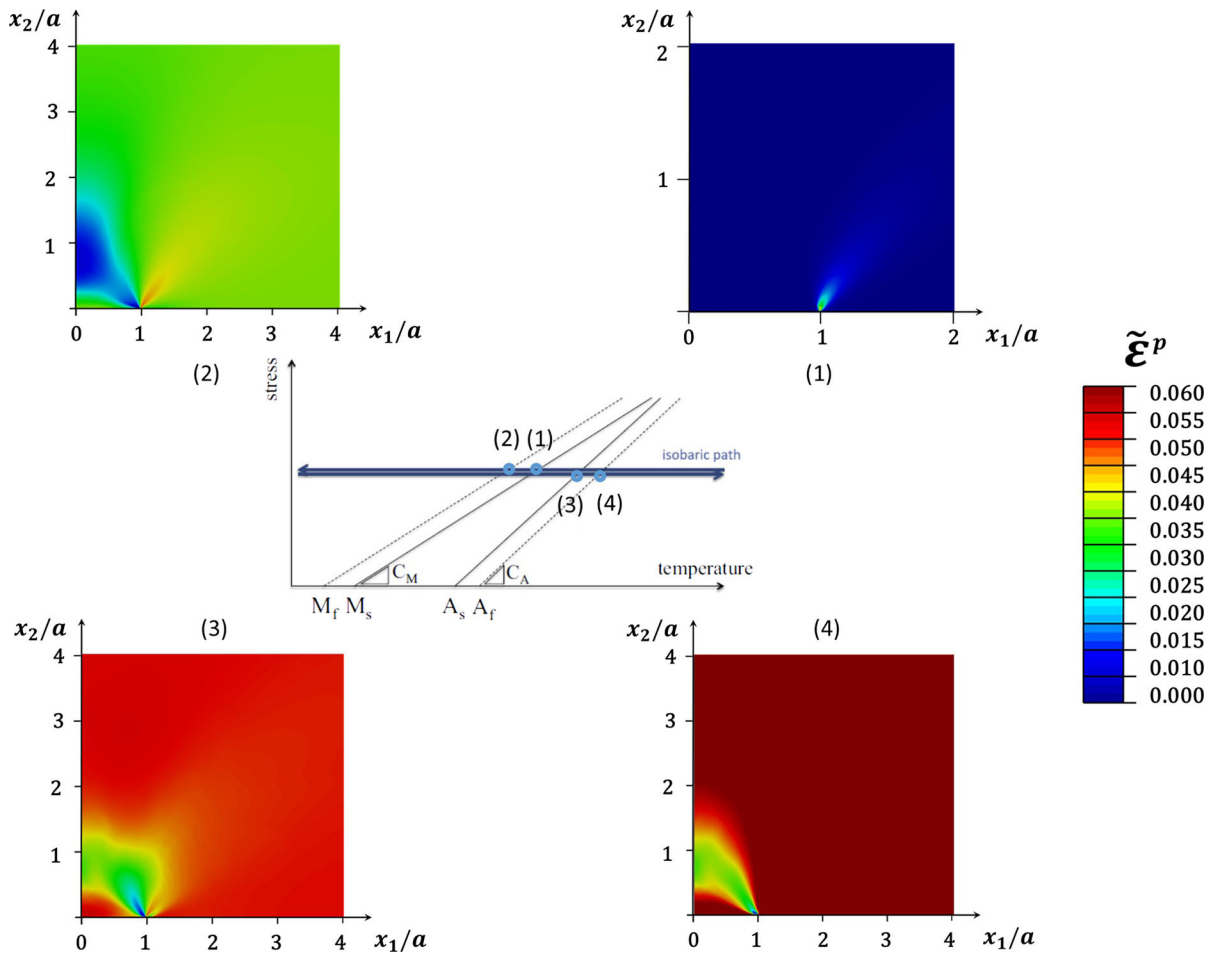
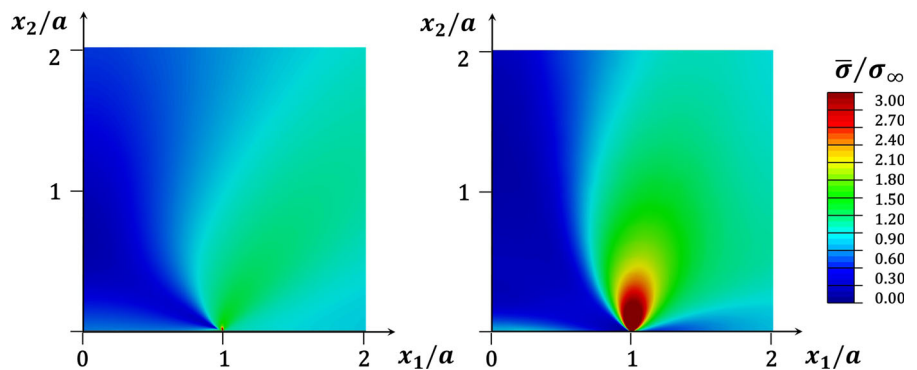


Fig. 6 Contours of equivalent plastic strain, $\tilde{\epsilon}^p = \sqrt{\frac{2}{3} \epsilon_{ij}^p \epsilon_{ij}^p}$, at different temperatures numbered on the stress–temperature phase diagram during the actuation loading. Note that the near-tip regions in which $\tilde{\epsilon}^p$ is depicted are of different sizes

Fig. 7 Von Mises stress distribution near the crack tip at $T = T_h$ prior to thermal cycling (left) and $T = T_c$ at the end of cooling (right).



a decrease of the energy release rate, again, overcoming the opposite effect of TRIP strains that continuously accumulate. At the end of the heating cycle, the G_I/G_∞ -value is higher than that at the beginning of

cooling, and this residual crack tip energy release rate is a result of permanent stress intensity enhancement due to the irreversibility of TRIP strains. Compared to previous studies (Jape et al. 2016; Baxevanis et al.

Fig. 8 Mean stress distribution near the crack tip at $T = T_h$ prior to thermal cycling (left) and $T = T_c$ at the end of cooling (right)

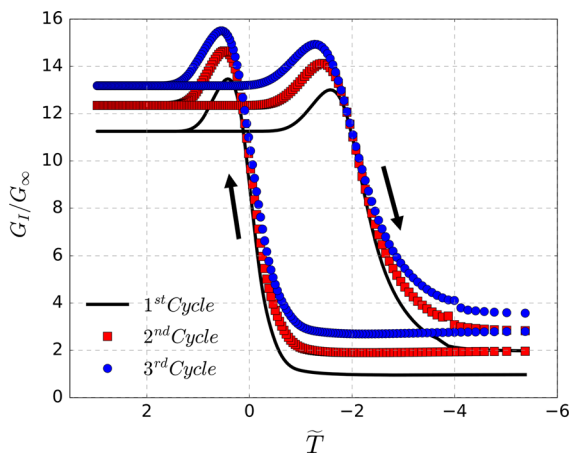
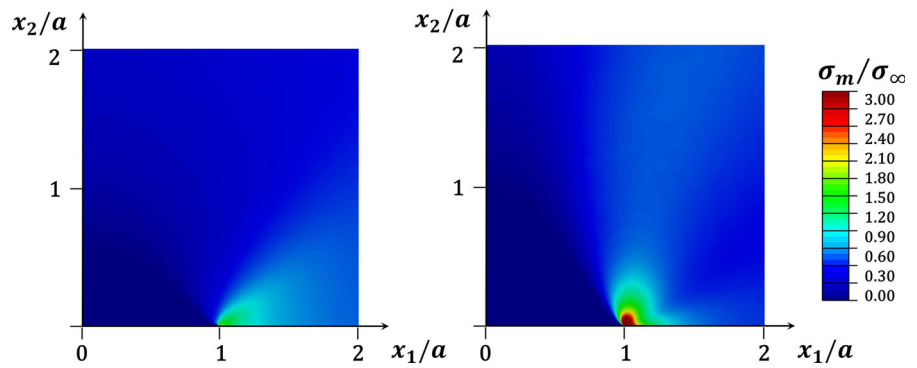


Fig. 9 Evolution of the normalized crack-tip energy release rate, G_I/G_∞ , versus uniform normalized temperature, $\tilde{T} = \left(\sqrt{H^{cur2} - 2\Delta S\rho\Delta s_o(T - M_s^o) - H^{cur}} \right) / \Delta S\sigma_\infty$, over three thermal cycles

2016) where the crack tip energy release rate variation during a thermal cycle remains unaltered in subsequent thermal cycles, the accumulation of TRIP over cycling in the present study further results in higher peak values from one cycle to another and a shift of the peak values towards lower temperatures (higher normalized ones) due to the corresponding shift that TRIP induces in the phase transition temperatures. An outcome of these results is that crack growth may be triggered, either in the first thermal cycle when the plane strain driving force for crack growth becomes equal to a material specific “critical” value, or in subsequent thermal cycles as a result of phase transformation and TRIP.

An experimental verification of the above findings has been given in a recent publication by Iliopoulos

et al. (in Press). During thermal cycling under a constant bias load as low as 50% of the load required for isothermal mechanical fracture at the highest temperature of the cycle, double-notched SMA specimens failed in most cases during the first cooling or after a limited number of cycles.

As already discussed, cyclic thermomechanical loading results in TRIP strain accumulation and in a progressive evolution of the transformation parameters induced by mainly TRIP driven microstructural modifications, i.e., shift of the phase transition temperatures, increase of the transformation hardening, and decrease of the width of the hysteresis loop and of the maximum transformation strain; all contributing to the stress redistribution that alters the driving force for crack growth. The direct contribution of the presence of TRIP strains to the driving force for crack growth is more pronounced than the implicit corresponding one arising from the microstructural modifications as can be deduced by comparing the subfigures in Fig. 10. In Fig. 10a, the variation of driving force for crack growth during three thermal cycles is depicted for TRIP accumulating in the material while the material parameters remain unaltered, and in Fig. 10b, the variation is depicted in the absence of TRIP but for evolving material properties. Note that in Fig. 10a, the G_I/G_∞ -peak values always occur at the same temperature while those in Fig. 10b shift to higher temperature values.

4.3 Stable crack growth

In this section, some aspects of the near-tip distribution of transformation and TRIP strain fields during crack growth are discussed. Crack advance initiates after a sufficient number of cycles, when

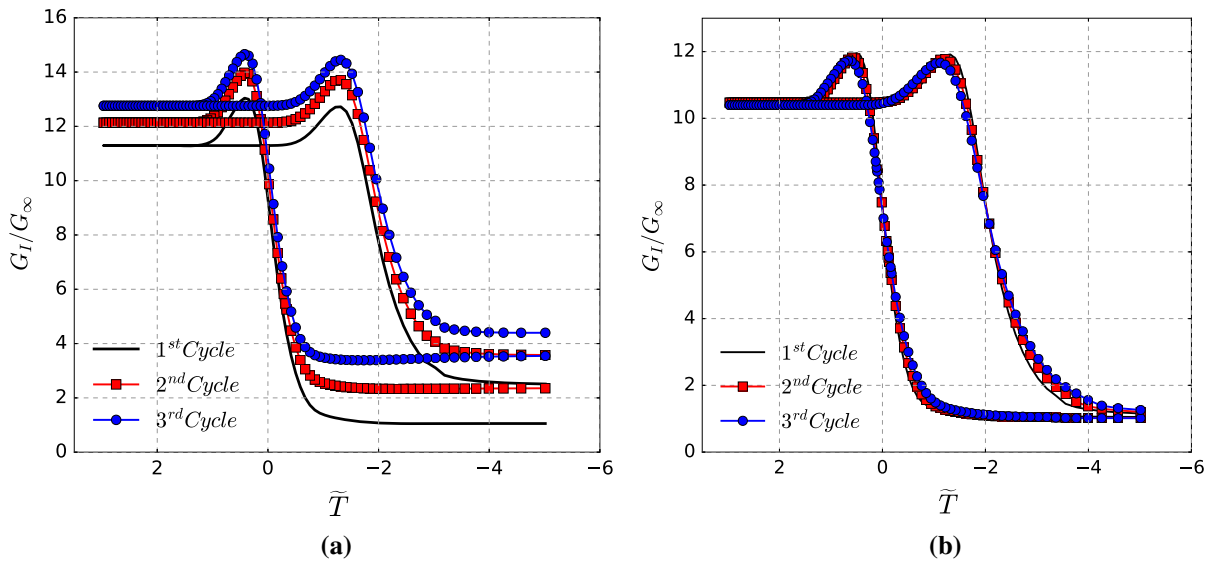
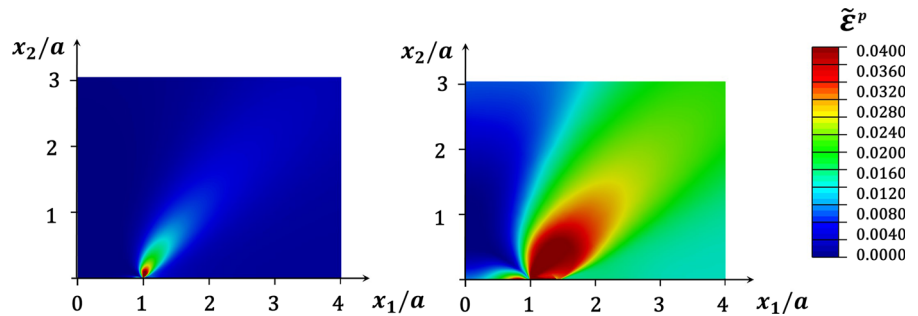


Fig. 10 Evolution of the normalized crack-tip energy release rate, G_I/G_∞ , versus uniform normalized temperature, $\tilde{T} = \left(\sqrt{H^{cur2} - 2\Delta S\rho\Delta s_o(T - M_s^o)} - H^{cur}\right) / \Delta S\sigma_\infty$, over three

thermal cycles in **a** the presence of TRIP for non-evolving material properties, and **b** in the absence of TRIP for evolving material properties. **a** Unaltered material properties **b** No TRIP

Fig. 11 Equivalent transformation induced plastic strain, $\tilde{\epsilon}^p$, in the vicinity of the crack tip **a** at the beginning of crack growth and **b** at the end of stable crack growth



the crack tip energy release rate increase due to the accumulated TRIP becomes equal to the critical value.

In Fig. 11, contours of TRIP strains in the vicinity of the advancing crack-tip are presented. As the crack advances, transformation and TRIP strains left in the wake of the advancing crack result, as already discussed, in shielding. Further cooling is required to compensate for this reduction in driving force by intensification of near-tip stresses due to further phase transformation and TRIP in front of the crack. The crack thus progresses in a stable manner resulting in a transformation/TRIP toughening behavior and an apparent “R-curve” behavior. Crack-resistance “R-curves” with normalized temperature on the vertical axis plotted

against normalized crack extension da/a on the horizontal axis for varying saturation level of TRIP strains are shown in Fig. 12. The “critical” energy release rate, G_{crit} , is assumed equal to $2G_\infty$ and crack advance initiates during cooling in the first thermal cycle. TRIP strains play a dual role during crack advance both by raising the driving force for crack growth when in front of the crack tip and by shielding the crack when left behind in the wake of the advancing crack. As expected, crack growth is triggered at higher temperature values for material systems experiencing higher TRIP strain magnitudes, i.e., TRIP promotes initiation of crack advance. The temperature change needed for reaching steady-state conditions from the initiation of crack advance is approximately $\Delta T = -6.85, -6.25$

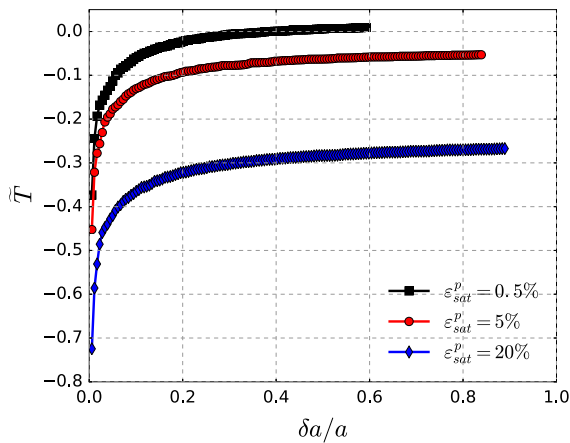


Fig. 12 Normalized temperature, $\tilde{T} = \left(\sqrt{H^{cur2} - 2\Delta S\rho\Delta s_o(T - M_s^o)} - H^{cur} \right) / \Delta S\sigma_\infty$, versus normalized crack growth, $\delta a/a$, for $G_{crit}/G_I = 2$ showing the crack resistance “R-curve” behavior. Black curve shows the case where the saturation level of the plastic strain is low enough to be negligible (0.5%); red curve shows the case where saturation plastic strain has a significant value (20%), whereas blue curve shows a case with intermediate level of saturation plastic strain (5%)

and -6.05 K, i.e., 0.45, 0.4 and 0.37 on the normalized temperature scale, for $\varepsilon_{sat}^p = 20, 5$ and 0.5% respectively. Moreover, the higher the TRIP values, the further the crack tip travels before steady state conditions are met. Thus, the shielding effect dominates and therefore TRIP is found not only to promote the initiation of crack advance but to also extend the stable crack growth regime.

5 Conclusions

Finite element calculations are carried out in Abaqus suite to investigate the mechanical fields near stationary and advancing cracks in SMAs subjected to actuation loading cycles. The prototype infinite center-crack problem is analyzed under a thermomechanical loading path which is an idealization of typical loading paths that utilize SMAs as actuators subjected to constant external mechanical loading under temperature variations. The driving force for crack growth is identified to be the crack-tip energy release rate, which is calculated using the virtual crack closure technique.

TRIP is found to affect both the driving force for crack growth and the crack growth kinetics in a fashion similar to phase transformation due to the induced stress redistribution that raises the driving force for crack growth when occurring in a fan in front of the crack tip and provides a shielding effect when occurring behind this fan. The accumulation of TRIP over cycling results in a higher driving force for crack growth from one cycle to another and a shift of the peak values towards higher temperatures due to the corresponding shift that TRIP induces in the phase transition temperatures. Thus, it is possible that crack growth may be triggered if the driving force for crack growth reaches a material specific “critical” value after a sufficient number of thermal cycles. With regard to growing cracks, stable growth occurs due to transformation and TRIP strains left in wake of the crack. TRIP strains play a dual role during crack advance both by raising the driving force for crack growth when in front of the crack tip and by shielding the crack when left behind in the wake of the advancing crack. The shielding effect dominates and therefore TRIP is found not only to promote the initiation of crack advance, but to also extend the stable crack growth regime.

Acknowledgements This material is based upon work supported by the Air Force Office of Scientific Research under Grant Number FA9550-15-1-0287.

References

- Abaqus (2015) Analysis user’s, manual. Dassault Systèmes of America Corp, Woodlands Hills
- Ardakani S, Hatefi AH, Mohammadi S (2015) Thermo-mechanically coupled fracture analysis of shape memory alloys using the extended finite element method. *Smart Mater Struct* 24:045031
- Baxevis T, Lagoudas DC (2012) A mode I fracture analysis of a center-cracked infinite shape memory alloy plate under plane stress. *Int J Fract* 175(2):151–166
- Baxevis T, Chemisky Y, Lagoudas DC (2012) Finite element analysis of the plane-strain crack-tip mechanical fields in pseudoelastic shape memory alloys. *Smart Mater Struct* 21(9):094012
- Baxevis T, Landis CM, Lagoudas DC (2013a) On the fracture toughness of pseudoelastic shape memory alloys. *J Appl Mech* 81(4):041005
- Baxevis T, Parrinello AF, Lagoudas DC (2013b) On the fracture toughness enhancement due to stress-induced phase transformation in shape memory alloys. *Int J Plast* 50:158–169

- Baxevanis T, Landis CM, Lagoudas DC (2014) On the effect of latent heat on the fracture toughness of pseudoelastic shape memory alloys. *J Appl Mech* 81(10):101006
- Baxevanis T, Parrinello AF, Lagoudas DC (2016) On the driving force for crack growth during thermal actuation of shape memory alloys. *J Mech Phys Solids* 89:255–271
- Birman V (1998) On mode I fracture of shape memory alloy plates. *Smart Mater Struct* 7:433–437
- Bo Z, Lagoudas DC (1999a) Thermomechanical modeling of polycrystalline SMAs under cyclic loading, Part II: material characterization and experimental results for a stable transformation cycle. *Int J Eng Sci* 37:1141–1173
- Bo Z, Lagoudas DC (1999b) Thermomechanical modeling of polycrystalline SMAs under cyclic loading, Part III: evolution of plastic strains and two-way shape memory effect. *Int J Eng Sci* 37:1175–1203
- Bo Z, Lagoudas DC (1999c) Thermomechanical modeling of polycrystalline SMAs under cyclic loading, Part IV: modeling of minor hysteresis loops. *Int J Eng Sci* 37:1205–1249
- Bo Z, Lagoudas DC (1999d) Thermomechanical modeling of polycrystalline SMAs under cyclic loading, Part I: theoretical derivations. *Int J Eng Sci* 37:1089–1140
- Boyd J, Lagoudas DC (1996) A thermodynamical constitutive model for shape memory materials, Part I: the monolithic shape memory alloy. *Int J Plast* 12(6):805–842
- Budiansky B, Hutchinson JW, Lambropoulos JC (1983) Continuum theory of dilatant transformation toughening in ceramics. *Int J Solids Struct* 19(4):337–355
- Cherkaoui M, Berveiller M, Sabar H (1998) Micromechanical modeling of martensitic transformation induced plasticity (TRIP) in austenitic single crystals. *Int J Plast* 14:597–626
- Creuziger A, Bartol LJ, Gall K, Crone W (2008) Fracture in single crystal NiTi. *J Mech Phys Solids* 56:2896–2905
- Daly S, Miller A, Ravichandar G, Bhattacharya K (2007) An experimental investigation of crack initiation in thin sheets of nitinol. *Acta Mater* 55:6322–6330
- Daymond MR, Young ML, Almer JD, Dunand DC (2007) Strain and texture evolution during mechanical loading of a crack tip in martensitic shape-memory NiTi. *Acta Mater* 55:3929–3942
- Desindes S, Daly S (2010) The small-scale yielding of shape memory alloys under mode III fracture. *Int J Solids Struct* 47:730–737
- Entchev P, Lagoudas DC (2004) Modeling of transformation-induced plasticity and its effect on the behavior of porous shape memory alloys, Part I: constitutive model for fully dense SMAs. *Mech Mater* 36:865–892
- Fischer F, Reisner G, Werner K, Tanaka E, Cailletaud T, Antretter G (2000) A new view on transformation induced plasticity (TRIP). *Int J Plast* 16:723–748
- Freed Y, Banks-Sills L (2007) Crack growth resistance of shape memory alloys by means of a cohesive zone model. *J Mech Phys Solids* 55:2157–2180
- Gall K, Yang N, Sehitoglu H, Chumlyakov Y (2001) Fracture of precipitated NiTi shape memory alloys. *Int J Fract* 109:189–207
- Gollerthan S, Young ML, Baruj A, Frenzel J, Schmahl WW, Eggeler G (2009) Fracture mechanics and microstructure in NiTi shape memory alloys. *Acta Mater* 57:1015–1025
- Hartl DJ, Lagoudas DC (2007) Aerospace applications of shape memory alloys. In: Proceedings of the institution of mechanical engineers. Part G: journal of aerospace engineering, SAGE pp 535–552
- Hazar S, Zaki W, Moumni Z, Anlas G (2015) Modeling of steady-state crack growth in shape memory alloys using a stationary method. *Int J Plast* 67:26–39
- Iliopoulos AP, Steuben JC, Kirk T, Baxevanis T, Michopoulos JG, Lagoudas DC, Thermomechanical failure response of notched NiTi coupons. *Int J Solids Struct–In Press*
- Irwin GR (1958) *Handbuch der Physik VI*. Springer, Berlin, pp 558–590 Ch. Fracture I
- Jape S, Baxevanis T, Lagoudas DC (2014) Stable crack growth during actuation in shape memory alloys. In: SPIE smart structures and materials + nondestructive evaluation and health monitoring. International Society for Optics and Photonics pp 905802(1–9)
- Jape S, Baxevanis T, Lagoudas DC (2016) Stable crack growth during thermal actuation of shape memory alloys. *Shape Memory Superelast* 2:104113
- Jape S, Baxevanis T, Parrinello AF, Lagoudas DC (2015) On the fracture response of shape memory alloy actuators. In: Proceedings of the TMS middle east: Mediterranean materials congress on energy and infrastructure systems (MEMA 2015). Wiley, pp 165–180
- Krueger R (2004) Virtual crack closure technique: History, approach, and applications. *Appl Mech Rev* 57(2):109–143
- Kumar PK, Lagoudas DC (2008) Shape memory alloys: modeling and engineering applications. Springer, New-York, pp 1–51 Ch. Introduction to Shape Memory Alloys
- Lambropoulos JC (1986) Shear, shape and orientation effects in transformation toughening. *Int J Solids Struct* 22:1083–1106
- Lexcellent C, Laydi MR, Taillebot V (2011) Analytical prediction of the phase transformation onset zone at a crack tip of a shape memory alloy exhibiting asymmetry between tension and compression. *Int J Fract* 169(1):1–13
- Liu Y, McCormick P (1994) Thermodynamic analysis of the martensitic transformation in Ti-Ni-I, effect of heat treatment on transformation behaviour. *Acta Metall Mater* 42:2401–2406
- Maletta C, Furguele F (2010) Analytical modeling of stress-induced martensitic transformation in the crack tip region of nickel-titanium alloys. *Acta Mater* 58:92–101
- Maletta C, Furguele F (2011) Fracture control parameters for NiTi based shape memory alloys. *Int J Solids Struct* 48:1658–1664
- Maletta C, Sgambitterra E, Fabrizio N (2016) Temperature dependent fracture properties of shape memory alloys: novel findings and a comprehensive model. *Sci Rep* 6:1–11
- Nespoli A, Besseghini S, Pittaccio S, Villa E, Viscuso S (2010) The high potential of shape memory alloys in developing miniature mechanical devices: a review on shape memory alloy mini-actuators. *Sens Actuators, A* 158(1):149–160
- Perkins J, Bobowiec P (1986) Microstructural effects of martensitic transformation cycling of a Cu-Zn-Al alloy: vestigial structures in the parent phase. *Metall Trans A* 17A:195–203
- Robertson SW, Metha A, Pelton AR, Ritchie RO (2007) Evolution of crack-tip transformation zones in superelastic Nitinol subjected to in situ fatigue: a fracture mechanics and synchrotron X-ray micro-diffraction analysis. *Acta Mater* 55:6198–6207

- Rybicki E, Kanninen M (1977) A finite element calculation of stress intensity factors by a modified crack closure integral. *Eng Fract Mech* 9:931–938
- Sreekumar M, Nagarajan T, Singaperumal M, Zoppi M, Molfino R (2007) Critical review of current trends in shape memory alloy actuators for intelligent robots. *Ind Robot* 34(4):285–294
- Stam G, van der Giessen E (1995) Effect of reversible phase transformations on crack growth. *Mech Mater* 21:51–71
- Ungár T, Frenzel J, Gollerthan S, Ribárik G, Balogh L, Eggeler G, (2017) On the competition between the stress-induced formation of martensite and dislocation plasticity during crack propagation in pseudoelastic NiTi shape memory alloys. *J Mater Res* 1–10. doi:[10.1557/jmr.2017.267](https://doi.org/10.1557/jmr.2017.267)
- Wang XM, Wang YF, Baruj A, Eggeler G, Yue ZF (2005) On the formation of martensite in front of cracks in pseudoelastic shape memory alloys. *Mater Sci Eng A* 394:393–398
- Xie D, Biggers S (2006) Progressive crack growth analysis using interface element based on the virtual crack closure technique. *Finite Elem Anal Des* 42:977–984
- Yan W, Mai Y (2006) IUTAM symposium on mechanics and reliability of actuating materials. Springer, Berlin, pp 217–226 Ch. Theoretical Consideration on the Fracture of Shape Memory Alloys
- Yi S, Gao S (2000) Fracture toughening mechanism of shape memory alloys due to martensite transformation. *Int J Solids Struct* 37:5315–5327
- Yi S, Gao S, Shen L (2001) Fracture toughening mechanism of shape memory alloys under mixed-mode loading due to martensite transformation. *Int J Solids Struct* 38:4463–4476